Atmospheric Research 166 (2015) 129–140

Contents lists available at ScienceDirect

Atmospheric Research

journal homepage: www.elsevier.com/locate/atmos

Uncertainties in anthropogenic aerosol concentrations and direct radiative forcing induced by emission inventories in eastern China

Wenyuan Chang [a,*], Hong Liao [a], Jinyuan Xin [a], Zhengqiang Li [b], Donghui Li [b], Xiaoye Zhang [c]

[a] State Key Laboratory of Atmospheric Boundary Layer Physics and Atmospheric Chemistry (LAPC), Institute of Atmospheric Physics, Chinese Academy of Sciences, Beijing 100029, China
[b] State Environmental Protection Key Laboratory of Satellites Remote Sensing, Institute of Remote Sensing and Digital Earth, Chinese Academy of Sciences, Beijing 100094, China
[c] Key Laboratory for Atmospheric Chemistry, Chinese Academy of Meteorological Sciences, Beijing 100081, China

ARTICLE INFO

Article history:
Received 15 January 2015
Received in revised form 29 May 2015
Accepted 18 June 2015
Available online 2 July 2015

Keywords:
Emission uncertainty
Aerosol concentration
Direct radiative forcing
ACCMIP

ABSTRACT

This study quantified the uncertainties in concentrations and direct radiative forcing of anthropogenic aerosols due to emissions in eastern China using a global chemistry–aerosol–climate model. The emission inventories included three global inventories, ACCMIP (Atmospheric Chemistry & Climate Model Intercomparison Project), EDGAR-HTAP (Emission Database for Global Atmospheric Research for Hemispheric Transport of Air Pollution), and EDGAR Version 4.2, and one regional INTEX-B (Intercontinental Chemical Transport Experiment—Phase B) inventory. The uncertainties (a percentage of the standard deviation divided by the mean value across the four inventories) in the regional surface-layer aerosol concentrations due to emissions were 3.9% in sulfate, 40.0% in nitrate, 18.4% in ammonium, 11.1% in POA, 16.7% in SOA and 15.4% in BC. Compared with the ACCMIP model results based on a uniform emission inventory, the impacts of emissions were smaller. One exception is the regional surface-layer nitrate concentration, which had comparable uncertainties due to the emissions (40.0%) and the models (43.8%) because of the complex nitrate chemistry and the highly uncertain NH_3 emission. The mean regional aerosol direct forcing at the top of the atmosphere between 1850 and 2006 was -3.6 Wm^{-2} under all-sky conditions and was enhanced up to -3.83 Wm^{-2} after the model assimilated the MODIS fine-mode aerosol optical depth (AOD). The impact of the assimilation of absorption AOD is discussed. The uncertainties in aerosol direct forcing were smaller than those of the ACCMIP inter-model results, but still significant. An accurate emission inventory is essential for quantifying the role of aerosols in regional climate.

1. Introduction

Direct radiative forcing (DRF) of aerosols, which involves the scattering or absorption of solar radiation by aerosols, has increased since the preindustrial era (Myhre et al., 2001, 2013a; Shindell et al., 2013; Lee et al., 2013). The Intergovernmental Panel on Climate Change (IPCC) Working Group I Fifth Assessment Report (WGI AR5) estimated a global mean aerosol direct forcing of -0.35 W m^{-2} in 2011 relative to 1750, with large uncertainties of -0.85 to $+0.15$ Wm^{-2} (Myhre et al., 2013a). Regional radiative forcing values could be larger than the global mean value and have higher uncertainties (Yu et al., 2006; Nakajima et al., 2007; Goto et al., 2011).

The uncertainties in aerosol DRF may be associated with differences in the physical and chemical processes in models. The AeroCOM (Aerosol Comparisons between Observations and Models) Phase II project (Kinne et al., 2006; Myhre et al., 2013b) and the ACCMIP (Atmospheric Chemistry & Climate Model Intercomparison Project) (Lamarque et al., 2013) evaluated the uncertainties resulting from the model differences under their own respective emission inventories, which were similar across the participating models. Sixteen of the AeroCOM Phase II global models predicted a global and annual mean aerosol optical depth (AOD) of 0.0295 with a standard deviation of 0.011 (Myhre et al., 2013b). Ten ACCMIP models predicted that the global normalized biases in the AOD against satellite datasets were between -30% and $+20\%$ (Shindell et al., 2013). The model diversities must take into account the aerosol burdens, mixture of black carbon with scattering aerosols, representation of the aerosol size distribution and lack of aerosol species (e.g., secondary organic aerosols, nitrate) (Kinne et al., 2006; Textor et al., 2007; Myhre et al., 2013b; Shindell et al., 2013).

Emission inventories influence aerosol simulations. Several historical bottom-up emission inventories developed for Asia (Streets et al., 2003; Ohara et al., 2007; Zhang et al., 2009; Lu et al., 2010; Lei et al., 2011) show considerable discrepancies in the emission amounts due to their differences in adopted emission factors and activity levels (e.g., energy consumption, industrial and agricultural production), as well as the complete level of revised emission sectors (Zhang et al., 2009; Lei et al., 2011). Zhao et al. (2011) estimated the uncertainties in emissions in China associated with the bottom-up methodology. They took Monte Carlo simulations by randomly taking emission factor and activity data 10,000 times under the parameters' probability

* Corresponding author at: LAPC, Institute of Atmospheric Physics, Chinese Academy of Sciences, Beijing 100029, China. Tel.: +86 10 62012063; fax: +86 10 62041393.
E-mail address: changwy@mail.iap.ac.cn (W. Chang).

http://dx.doi.org/10.1016/j.atmosres.2015.06.021
0169-8095/

distributions that were created based on the field measurements in year 2005. They found that the uncertainties in emissions were −14% to 13% for sulfur dioxide (SO_2), −13% to 37% for nitrogen oxides (NO_x), −25% to 136% for black carbon (BC) and −40% to 121% for organic carbon (OC). Granier et al. (2011) investigated several global and regional emission inventories assessed for 1980–2010 and claimed that improved quantification was needed for emissions in central Europe, India and China. According to 8 inventories for BC, CO and NO_x and 10 inventories for SO_2, the emission ratios in year 2000 of the highest to the lowest in China were 2.12 for BC, 1.43 for carbon monoxide (CO), 1.31 for NO_x and 1.78 for SO_2.

Thus far, few studies have examined the uncertainties in emission inventories in aerosol simulations, and those existing were from a global perspective. Textor et al. (2007) analyzed the global mean AeroCOM phase I results and concluded that the uncertainties in global aerosol concentrations were dependent on the model's chemical and physical processes, except the uncertainty in emissions. Stier et al. (2006) switched off the anthropogenic emissions to learn the nonlinear response of the global aerosol mass concentration and number burden due to the microphysical change in aerosol aging and geographical shifts in emission source. Lee et al. (2011) examined the sensitivity of simulated CCN to emissions of sulfate particulate, sulfur, and sea spray, as well as that of simulated CCN to a few physical and chemical parameters (i.e., aqueous phase oxidation activation diameter, mass accommodation coefficient, sulfuric acid nucleation threshold, nucleation critical cluster size and cloud nucleation scavenging diameter). They found that uncertainties in sulfur emissions contributed to 80% of the CCN concentration variance in polluted environment.

Chinese anthropogenic emissions account for 66% of SO_2, 57% of NO_x, 56% of CO, 62% of BC and 49% of OC in Asian emissions (Zhang et al., 2009). The major emission sources are located in populated eastern China, where the regional aerosol direct forcing has been extensively estimated for certain species of sulfate (Giorgi et al., 2002; Wang et al., 2003), nitrate (Wang et al., 2010b; Zhang et al., 2012a; Li et al., 2014; Park et al., 2014b) and carbonaceous particulates (Wu et al., 2008; Zhuang et al., 2011), as well as their mixtures (Chang et al., 2009; Zhang et al., 2012b). These studies were based on emission driving chemistry-climate models, but discussion of the impact of emission inventories on regional aerosol simulation is rare.

The goal of this study is to investigate the sensitivities of anthropogenic aerosol concentrations, aerosol optical properties and aerosol DRF values over eastern China to four emission inventories from ACCMIP, EDGAR, HTAP and INTEX-B. Because the global models tend to underestimate eastern Asian AOD (Shindell et al., 2013), we constrained the DRF by assimilating the satellite- and ground-based fine-mode AOD through optimal interpolation (Collins et al., 2001; Chung et al., 2010; Park et al., 2014a). Section 2 describes the global model and emission inventories. The model results for aerosol concentrations, optical properties and DRF are presented in Section 3. Section 4 discusses AAOD, and Section 5 summarizes the work in the conclusion.

2. Methodology

2.1. The CACTUS model

Aerosol concentrations and DRF were simulated using the fully coupled tropospheric chemistry-aerosol-climate model within the GISS (Goddard Institute for Space Studies) GCM II′ (Liao et al., 2004; Liao and Seinfeld, 2005; Liao et al., 2006, 2009), which was developed by the National Aeronautics and Space Administration (NASA) project, Chemistry, Aerosols, and Climate: Tropospheric Unified Simulation (CACTUS). The model includes a detailed simulation of tropospheric O_3–NO_x–hydrocarbon chemistry, as well as of sulfate, nitrate, ammonium, BC, primary organic aerosols (POA), secondary organic aerosols (SOA), sea salt and mineral dust. The GISS GCM II′ has a horizontal resolution of 4° latitude by 5° longitude, with 9 vertical layers from the surface to 10 hPa. The CATUS model is coupled with a Q-flux ocean (Hansen et al., 1984). In the Q-flux ocean, ocean heat transport is held constant but sea surface temperatures and ocean ice respond to changes in climate.

The model assumes lognormal size distributions for different dry aerosol species. The water uptake by aerosols is calculated by the online thermodynamics equilibrium module ISORROPIA (Nenes et al., 1998). Aerosol species are assumed to be internally mixed and the refractive index of the mixed aerosol is calculated by the volume-weighted average of the refractive index of each aerosol component and associated water. The wavelength dependent aerosol optical properties (extinction coefficient, scattering coefficient, and asymmetric factor) are calculated by using the Mie theory.

2.2. Emission inventories

The aerosol simulations were based on anthropogenic, biomass burning, and natural emissions in 2006. The natural emissions include NO_x from lightning and soil, biogenic hydrocarbons, sea salt and dimethyl sulfide from the oceans, which are calculated online depending on the meteorological conditions (Liao et al., 2004, 2006). The anthropogenic and biomass burning emission inventories are briefly described below.

2.2.1. ACCMIP emissions

The ACCMIP historical emissions inventory was established for the ACCMIP project (Lamarque et al., 2010) in support of the climate model experiments for the IPCC AR5. It contains reconstructed historical emission datasets from 1850 to 2000 for every 10 years. The inventory has emissions from 12 sectors with a horizontal resolution of 0.5° × 0.5°. The chemical species include methane, CO, NO_x, SO_2, ammonia (NH_3), BC, POA and non-methane volatile organics. For 2006, emissions were interpolated between the annual emissions in 2000 and 2010 using the Representative Concentration Pathway (RCP) 4.5 (van Vuuren et al., 2011).

2.2.2. EDGAR-HTAP emissions

The EDGAR-HTAP (Emission Database for Global Atmospheric Research for Hemispheric Transport of Air Pollution) global emission inventory (hereafter referred to as HTAP) is the compilation of different official or scientific inventories at the national or regional scale. The emissions in China were compiled from GAINS-China datasets, and Asian emissions outside of China were from REAS (Regional Emission inventory in Asia) (Ohara et al., 2007). This dataset includes anthropogenic emissions of SO_2, NO_x, CO, NH_3, BC and OC. The HTAP inventory has two versions. Version 1 has annual emissions from 2000–2005, and version 2 has emissions in 2008 and 2010. For 2006, emissions were interpolated between 2005 and 2008.

2.2.3. EDGAR Version 4.2 emissions

The global EDGAR anthropogenic emission dataset (version 4.2) was compiled by the European Commission, Joint Research Center (JRC)/Netherlands Environmental Assessment Agency. This dataset has only emissions of SO_2, NO_x, CO, and NH_3 from anthropogenic and biomass burning sectors and includes no carbonaceous aerosol emissions. The annual emissions have a resolution of 0.1° × 0.1° and cover the period from 1970 to 2008.

2.2.4. INTEX-B emissions

The Asian INTEX-B emission inventory was established in 2006 for the Intercontinental Chemical Transport Experiment—Phase B (INTEX-B) project. It contains anthropogenic emissions of SO_2, NO_x, CO, BC, POA, PM_{10}, $PM_{2.5}$ and VOCs (volatile organic compounds) and has no NH_3 emission. Biomass burning emissions are also absent. This inventory has a horizontal resolution of 0.5° × 0.5° and covers anthropogenic

emissions in China, Mongolia, Korea, Japan, India and Indonesia (Zhang et al., 2009).

Four simulations based on each emission inventory were performed. Because not all of the inventories contained all of the species or sectors required by the model, they collaborated with each other in the simulations. The HTAP inventory contained only anthropogenic emissions and was combined with the biomass burning emission inventory of Global Fire Emission Database (GFED) version 3.1. The EDGAR inventory lacked carbonaceous aerosol emissions and was combined those from the HTAP and GFED inventories. Based on the EDGAR inventory, the Asian emissions were further replaced by the INTEX-B inventory. The ACCMIP inventory contains all of the precursors and sectors and was used exclusively in the model. For convenience, we named each simulation based on the name of the inventory providing the anthropogenic SO_2 emission for China. All of the anthropogenic emissions were reported as annual mean values, except for the biomass burning and natural emissions calculated online, which had monthly variations in the model.

Table 1 lists the annual emission amounts of aerosol precursors and primary aerosols over eastern China (100°–120°E, 24°–44°N). We defined an uncertainty as a percentage of the standard deviation divided by the mean value across the four inventories/simulations. Fig. 1 shows the geographical distributions of the annual and average emissions across the inventories and their uncertainties. The four inventories consistently showed large emission amounts in eastern China. All emissions had maximum values in the North China Plain, which is consistent with the distributions of urbanization and population. CO had the largest emissions, and SO_2 was the second largest because coal combustion is a primary emission source in this country. NO_x was the third most abundant emission species due to the rapid increase in vehicles that is in turn increasing pollution (Zhang et al., 2009).

In eastern China, CO emission had the largest uncertainty (27.9%) because EDGAR contains low CO emissions from the biomass burning and fossil fuel sectors. NH_3 had the second largest uncertainty (18.4%) partly because ammonia volatilization (particularly in fertilizer applications) is strongly dependent on the varying soil acidity and ambient temperature (Huang et al., 2012; Zhou et al., 2015). Meanwhile, an inventory may not contain all relevant sectors. The HTAP NH_3 is comprised solely of the agricultural and waste-handling sectors, while EDGAR and ACCMIP additionally contain NH_3 emissions from the industrial, energy and transportation sectors. Carbonaceous aerosol emissions had comparable uncertainties (i.e., 15.4% for BC and 11.9% for OC) that are associated with the lack of statistical data on applications of combustion technology (e.g., residential burning of raw coal or briquettes), fuel type (e.g., biofuel, coal, diesel) and the amount of biomass burning in China (Zhang et al., 2009; Qin and Xie, 2011). Information on the industrial and transportation sectors is relatively well known (Zhao et al., 2011). Thus, SO_2 and NO_x had the lowest emission uncertainties of 5.3% and 6.6%, respectively. Additionally, there were a few high emission uncertainties from remote areas (e.g. Siberia, Tibetan Plateau) because of a few differences in biomass burning emissions and the low emission levels causing even these slight differences noticeable.

2.3. Measurement datasets

The measurements used to evaluate the model's aerosol concentrations were the two-year (2006–2007) monthly averages of surface-layer aerosol concentrations from the Chinese Atmosphere Watch Network (CAWNET) affiliated with the Chinese Meteorological Administration. The datasets contained PM_{10} concentrations of sulfate, nitrate, ammonium, BC, OC and mineral dust, as well as a derived mass concentration of SOA (Zhang et al., 2012c). The aerosol concentrations, except for dust, were multiplied by 0.6 to represent the fine-mode particulate concentration, as suggested by Zhang et al. (2004). Fig. 2 shows the 14 site locations.

The 550 nm AOD datasets were from the hand held hazemeter measurements in 2005–2007 at 20 sites of the China Sun Hazemeter Network (CSHNET) (Xin et al., 2007; Wang et al., 2011). Because it is difficult to depict uneven aerosol distributions using point observations, we used additional 2012–2014 sun-photometer measurements from 5 sites that were operated by the Institute of Remote Sensing and Digital Earth, Chinese Academy of Sciences, and combined the two datasets to nudge the satellite AOD in spite of their temporal mismatch. Xin et al. (2011) studied the AOD monthly variations from 2004–2010 in northeastern China. They found that the magnitudes of the linear changes in AOD from 2004–2010 were generally less than 0.05 (Figures 2 to 5 in Xin et al., 2011). Therefore, the use of 2012–2014 datasets should not compromise our conclusions. Fig. 4 shows the 25 site locations.

We applied two monthly satellite datasets from 2006: the Aqua MODerate Resolution Imaging Spectroradiometer (MODIS) Collection 051 (level 3, 550 nm AOD) and the Terra Multi-angle Imaging SpectroRadiometer (MISR) (555 nm AOD). They were downloaded from the NASA Giovanni website and had a global resolution of $1^\circ \times 1^\circ$. Extensive studies have validated the satellite AOD datasets in China. Wang et al. (2010a) demonstrated that the 2004–2007 MODIS C005 aerosol products underestimated the AOD over China by approximately 0.03 to 0.07. Liu et al. (2010) found that the 2004–2006 MISR AOD had a systematic underestimation when the AOD value was greater than 0.5. Cheng et al. (2012) claimed that both MODIS and MISR showed lower retrieval accuracies in China than in the U.S., Europe and North Africa. Therefore, the satellite AOD was first nudged to the ground-based AOD observations at the 25 sites before the model assimilation.

2.4. Optimal interpolation (OI) methodology

The assimilation method is optimal interpolation (OI), which is to calculate error-weighted average between two datasets. Specifically,

Table 1
Annual emissions of aerosol precursors and aerosols in eastern China (100°–120°E, 24°–44°N) in 2006 in the four emission inventories. The mean and one standard deviation (Std.) were calculated based on the four emission inventories.

Emission inventories	SO_2 $Tg(SO_2)$	NH_3 $Tg(NH_3)$	NO_x Tg(NO)	CO Tg(CO)	OC Tg(C)	BC Tg(C)
ACCMIP	21.35	4.33	7.85	99.96	2.71	1.43
HTAP[a]	22.01	6.82	8.37	119.51	2.13	1.07
EDGAR[b]	22.32	5.53	7.68	60.49	2.13	1.07
INTEX-B[c]	24.12	5.53	8.87	119.87	2.41	1.36
Mean ± Std	22.45 ± 1.18	5.55 ± 1.02	8.19 ± 0.54	99.96 ± 27.91	2.35 ± 0.28	1.23 ± 0.19
Std/Mean × 100%	5.3%	18.4%	6.6%	27.9%	11.9%	15.4%

[a] The HTAP inventory consisted of anthropogenic emissions from the HTAP inventory and biomass burning emissions from the GFED inventory.
[b] The EDGAR inventory had emissions of SO_2, NH_3, NO_x and CO from the anthropogenic and biomass burning sectors. The emissions of carbonaceous aerosols (BC and OC) were taken from the HTAP anthropogenic emission inventory and the GFED biomass burning emission inventory.
[c] The INTEX-B inventory only included Asian emissions of SO_2, NO_x, CO, BC and OC. Emissions outside of Asia were taken from the case of EDGAR[b].

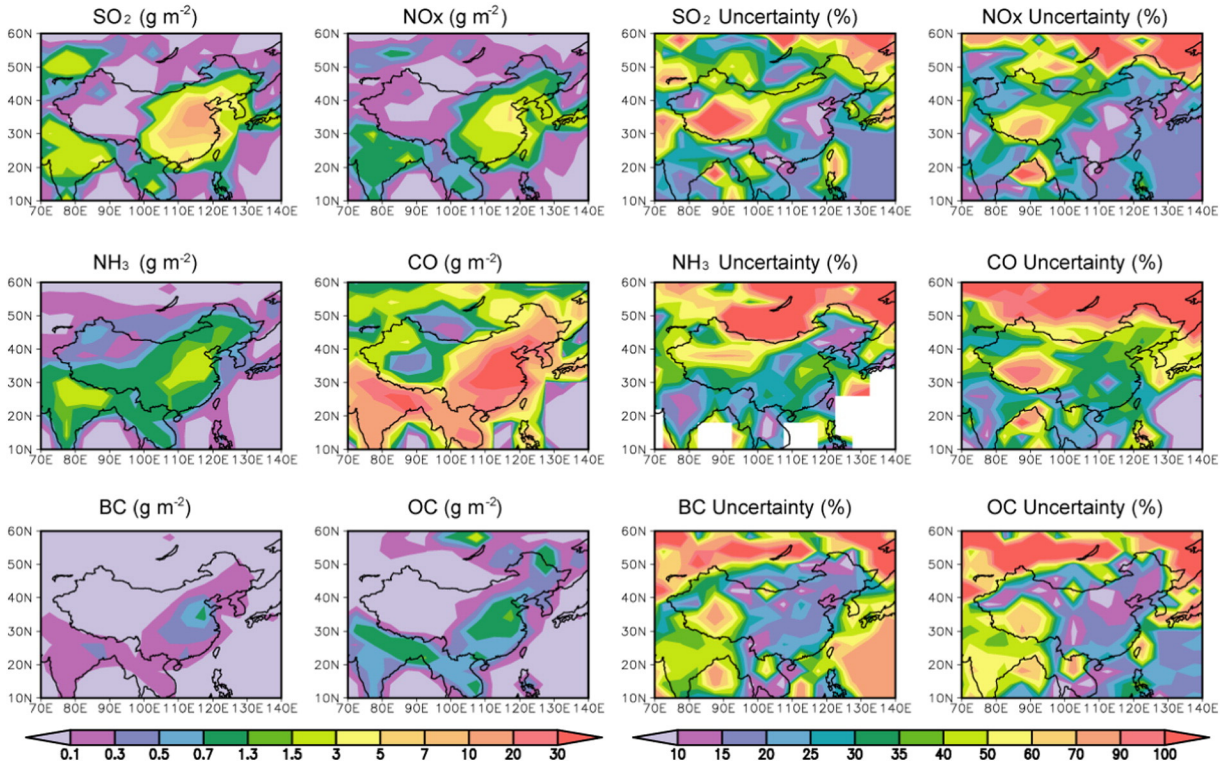

Fig. 1. Annual emissions of aerosol precursors and aerosols (including anthropogenic and biomass burning emissions) and their uncertainties (ratio of the standard deviation to the mean value as a percentage) across the 2006 emission inventories of ACCMIP, HTAP, EDGAR and INTEXB in China. The units of emissions of SO_2, NO_x, NH_3, CO, BC and OC are g (SO_2, NO_x, NH_3, CO, C, C) m^{-2} $year^{-1}$, respectively.

the model AOD (τ_m') was nudged by the AOD difference between the observation (τ_o) and model (τ_m) as the follow:

$$\tau_m' = \tau_m + \boldsymbol{K}(\tau_o - \boldsymbol{H}\tau_m) \quad (1)$$

where $\boldsymbol{K}$ is a weight operator determining the specific correction at each model grid. It is based on an observation error ($\boldsymbol{O}$) and a background error (i.e., model error, $\boldsymbol{B}$):

$$\boldsymbol{K} = \boldsymbol{B}\boldsymbol{H}^T\left(\boldsymbol{H}\boldsymbol{B}\boldsymbol{H}^T + \boldsymbol{O}\right)^{-1}. \quad (2)$$

The $\boldsymbol{H}$ is a linear operator transferring the model value/error into the observation locations. In our case, the observation AOD was remapped into the model resolution, which simplifies the $\boldsymbol{H}$ operator to the identity matrix $\boldsymbol{I}$. The observation error consists of a measurement error (e_o) and a representative error (e_r). The former is the intrinsic error of the observation, and the latter denotes the capability of a fine-grid observation to describe aerosols over a large model grid. The observation error covariance between locations is ignored, and the final observation error matrix $\boldsymbol{O}$ is:

$$\boldsymbol{O} = (e_o^2 + e_r^2)\boldsymbol{I}. \quad (3)$$

The background error field $\boldsymbol{B}$ denotes the spatial relationship of the background error (e_m):

$$\boldsymbol{B}(lon, lat) = e_m^2 \exp\left(-\frac{d^2}{2l^2}\right) \quad (4)$$

where d is the distance between the two model grids, and l is the horizontal correlation length-scale of error that is typically 100 km (Collins et al., 2001).

The OI calculation was performed twice. Firstly, to create a best observation, the satellite AOD was nudged to the ground-based AOD. The satellite dataset was regarded as a "model" result and was linearly interpolated to the ground site locations. The satellite AOD error was the MODIS retrieval uncertainty over land, $e_o = 0.05 \pm 0.15 \times \tau_o$ (Remer et al., 2005). The ground-based observation error was 0.05. Since we care about the anthropogenic aerosols, the nudged AOD observation was scaled to attain the fine-mode AOD (fAOD) based on the median ratio of anthropogenic AOD to total AOD across the five ACCMIP models (i.e., CICERO-OsloCTM2, GFDL-AM3, GISS-E2-R, GISS-TOMS, HadGEM2). Secondly, the nudged observation was assimilated with the CACTUS model result. The observation error was still the MODIS retrieval uncertainty and the representative error was the standard deviation of fAOD over a fine satellite grid (1° × 1°) in a coarse model grid (4° × 5°). The model error was the standard deviation of fAOD across the five ACCMIP models. The adjustment of the model fAOD was distributed to fAOD at each model layer based on the weights calculated from the layer fAOD variation across the five ACCMIP models, after which the new fAOD was ready for the aerosol forcing estimation.

Absorption AOD (AAOD) in 2006 derived from the Ozone Monitor Instrument (OMI) Level 2 on the Aqua satellite was also considered, but the OI calculation for AAOD was difficult because of the lack of quantitative estimation on the error in the AAOD observations. We firstly show the impacts of fAOD assimilation in Section 3.2.4 and discussed the impact of AAOD assimilation in Section 4.

2.5. The ACCMIP model data

The ACCMIP model results were applied in this study to show the agreement of our model with other global models, identify the significance of the impact of emissions through comparison of the diverse model results due to the model differences, and estimate the inter-

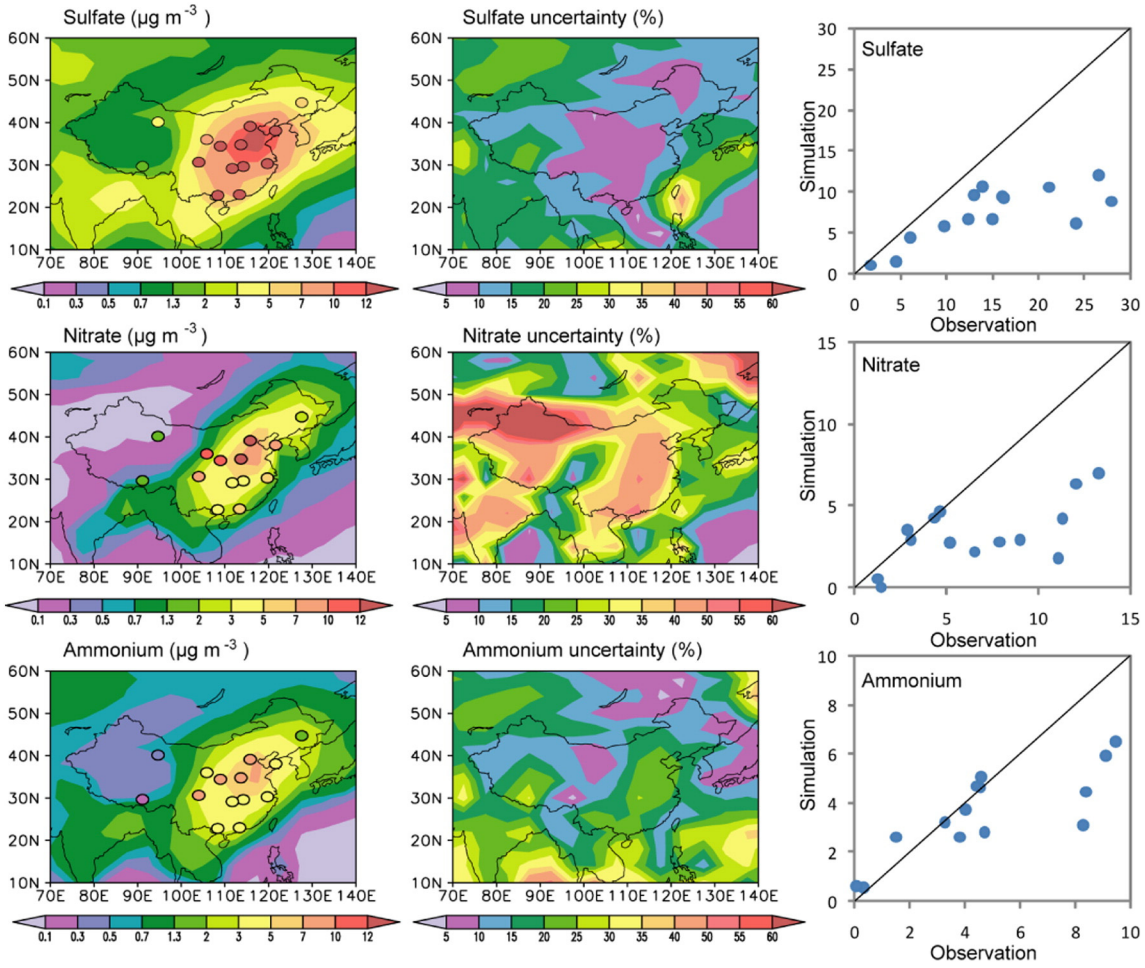

Fig. 2. Simulated annual mean surface-layer concentrations of sulfate, nitrate and ammonium (μg m^{-3}) in China and their uncertainties (ratio of the standard deviation to the mean value as a percentage) across the 2006 emission inventories of ACCMIP, HTAP, EDGAR and INTEX-B. The circles in the left column show the magnitudes and locations of the CAWNET measurements.

model variation in AOD used as model error for the OI assimilation as shown in Section 2.4. Table 2 shows the global burdens of aerosol species, fAOD excluding AOD of dust and sea salt, and anthropogenic absorption AOD (AAOD) in the models. In general, CACTUS provided the global aerosol burdens, and fAOD and AAOD were within the ranges of the ACCMIP models, but near the low end.

Table 2
Global burdens (Tg) of aerosol species, fine-mode aerosol optical depth (fAOD) and anthropogenic (Anth.) absorption AOD (AAOD) simulated in this work using the ACCMIP emissions for the year 2000. The maximum (Max.), minimum (Min.), mean value, one standard deviation (Std), and uncertainty (ratio of std to mean value in percentage) of the ACCMIP model results in 2000 are also listed for comparison. The POA and SOA in this and the latter tables are in units of organic matter.

			Global Budget (Tg)				Anth. fAOD	Anth. AAOD
	Sulfate	Nitrate	Ammonium	POA	SOA	BC		
CACTUS model	1.23	0.21	0.38	0.55	0.31	0.09	0.04	0.002
ACCMIP models								
Max.	4.44	7.58	0.92	1.58	1.09	0.31	0.13	0.005
Min.	1.24	0.08	0.19	0.51	0.08	0.08	0.04	0.001
Mean	2.07	3.25	0.72	1.00	0.53	0.15	0.06	0.004
Std	0.88	3.55	0.56	0.36	0.44	0.07	0.03	0.002
Std/Mean × 100%	42.5%	109.2%	77.8%	36.0%	83.0%	46.7%	50%	50%

3. Results

3.1. Evaluation of model performances in eastern China

3.1.1. Surface-layer aerosol concentrations

Figs. 2 and 3 show the simulated annual mean surface-layer aerosol concentrations in China and their uncertainties. CACTUS reasonably reproduced the maximum concentrations in the north and captured the dominant component of sulfate. However, the aerosol concentrations were underestimated. The mean biases at the CAWNET sites were −51.3% to −44.7% for sulfate, −71.6% to −29.9% for nitrate, −70.8% to −62.5% for ammonium, −54.8% to −43.5% for POA, −86.7% to −85.5% for SOA, and −61.1% to −50.5% for BC (Table 3).

The negative biases reported above were caused in part by the coarse model resolution missing the subgrid variations in precursors and particulates. We found that the significant low biases were also in the ACCMIP model results (negative biases larger than 50%) though the ACCMIP simulations used emissions of 2000, while the measurements were taken in 2006. To isolate the impact of increased emissions over 2000–2006, we performed a CACTUS simulation by using the ACCMIP emissions for 2000 and found that the regional aerosol increases over 2000–2006 were no more than 2 μg m^{-3} (Table 3), lower than the model biases in the ACCMIP model simulations. It suggests that the low biases are not accident in CACUTS but are common in global models. Besides to the resolution, the transport and deposition of

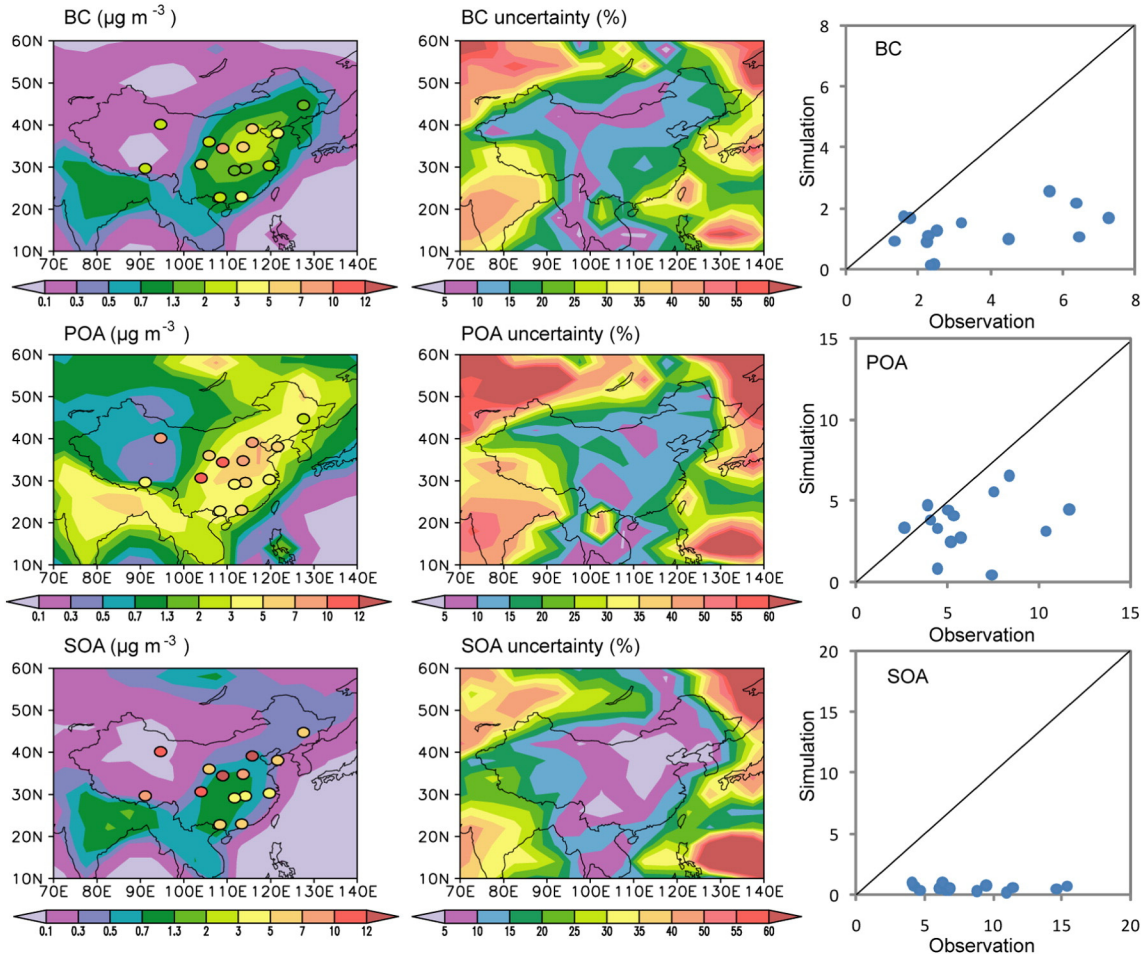

Fig. 3. Same as Fig. 2, but for the surface-layer concentrations of BC, POA and SOA (μg m^{-3}).

aerosols depend on simulated climate (Zhang et al., 2010) and the chemistry scheme in the model may need to be improved (Wang et al., 2014; Zheng et al., 2015). To examine the impacts of the low biases in concentrations, we will calculate aerosol radiative forcing by using assimilated AOD in Section 3.2.4.

3.1.2. Aerosol optical properties

Fig. 4 compared the simulated annual mean values of single scattering albedo (SSA), AOD and AAOD with the ground-based measurements (CSHNET sites plus 5 sunphotometer sites operated by the Institute of Remote Sensing and Digital Earth, Chinese Academy of Sciences). With all aerosol species considered (SO_4^{2-}, NO_3^-, NH_4^+, OC, BC, sea salt, and mineral dust), the simulated AOD and AAOD were high whereas SSA values were low over Northern China, as a result of the strong anthropogenic emissions and high mineral dust concentrations in this region. Compared with measurements at the 25 sites, the simulated AOD exhibited biases of −0.04 (−9.8%). The simulated average AOD over eastern China was 0.37, which falls within the AOD ranges of 0.26 from MISR and 0.39 from MODIS. Despite of the good overall performance, the negative biases in AOD were larger than 0.2 over central China, because the simulated mineral dust concentrations were low and anthropogenic aerosols were underestimated over there.

Over eastern China, the regional mean AAOD was simulated to be 0.027, which agreed closely with OMI AAOD of 0.025. At the 25 sites, simulated AAOD showed average biases of −0.01 (−26.9%). The average SSA at 550 nm at the CSHNET sites was observed to be 0.86 in 2005–

Table 3
Comparisons of the simulated aerosol concentrations (μg m^{-3}) from the CACTUS model with the CAWNET observations of aerosol mass concentrations reduced by 40%. For each emission inventory, the model bias is given as $1/14 \times \sum_{i=1}^{14}(c_i^{mod} - c_i^{obs})/c_i^{obs} \times 100$ %, where c_i^{mod} and c_i^{obs} are the modeled and observed concentrations at station i, respectively.

	Sulfate	Nitrate	Ammonium	POA	SOA	BC
Observation	15.0	6.7	4.8	6.2	8.3	3.6
Based on emissions in 2000						
ACCMIP	−9.2 (−61.3%)	−5.2 (−77.6%)	−3.5 (−72.9%)	−3.3 (−53.2%)	−7.2 (−86.7%)	−2.3 (−63.9%)
Based on emissions in 2006						
ACCMIP	−7.7 (−51.3%)	−4.8 (−71.6%)	−3.0 (−62.5%)	−2.7 (−43.5%)	−7.1 (−85.5%)	−1.8 (−50.5%)
HTAP	−6.9 (−46.0%)	−2.0 (−29.9%)	−3.4 (−70.8%)	−3.2 (−51.6%)	−7.2 (−86.7%)	−2.2 (−61.1%)
EDGAR	−7.3 (−48.7%)	−2.8 (−41.8%)	−3.3 (−68.8%)	−3.4 (−54.8%)	−7.2 (−86.7%)	−2.1 (−58.3%)
INTEX-B	−6.7 (−44.7%)	−3.3 (−49.3%)	−3.4 (−70.8%)	−3.2 (−51.6%)	−7.1 (−85.5%)	−2.2 (−61.1%)

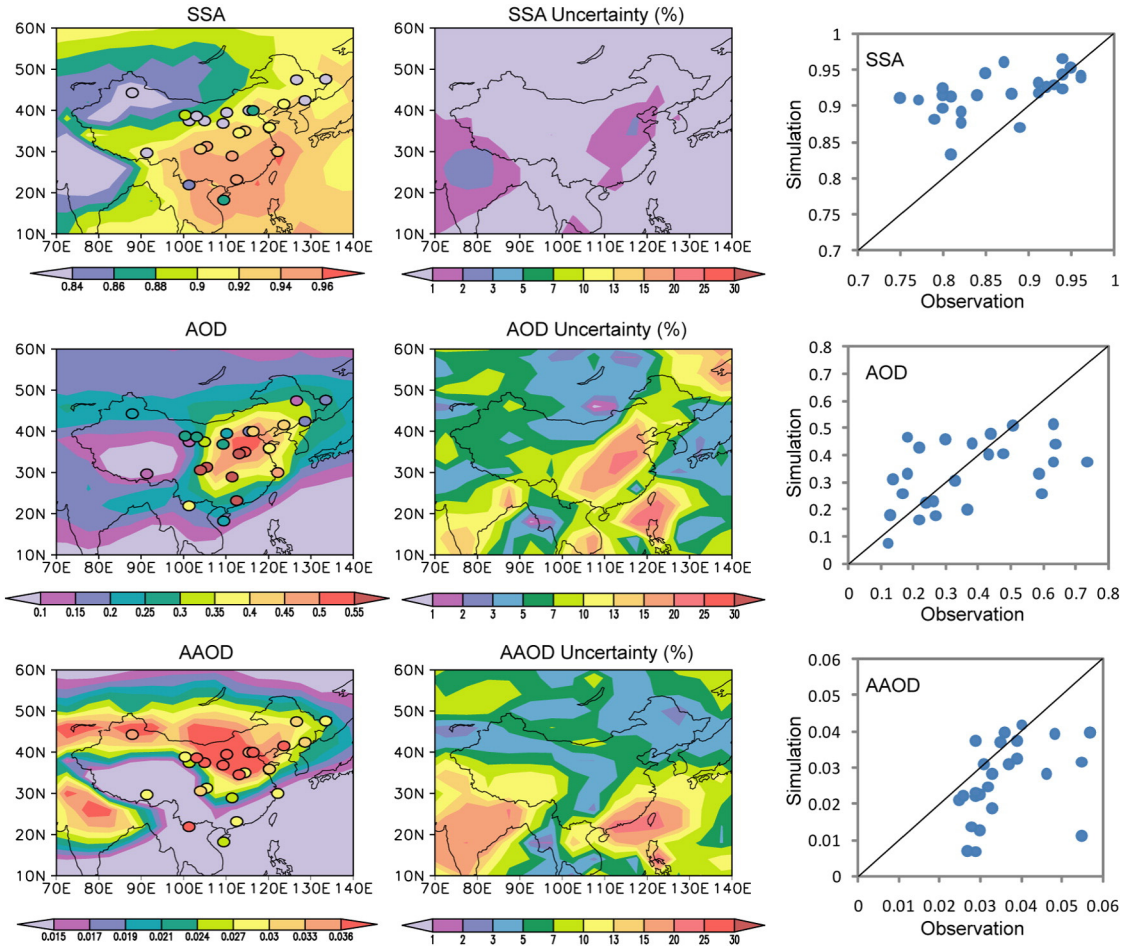

Fig. 4. Simulated annual mean values of single scattering albedo (SSA), total aerosol optical depth (AOD), and absorption AOD (AAOD) in China and their uncertainties (ratio of the standard deviation to the mean value as a percentage) across the 2006 emission inventories of ACCMIP, HTAP, EDGAR and INTEX-B. The circles in the left panels show the locations and magnitudes of the ground-based observations. The calculations of AOD, AAOD, and SSA accounted for all aerosol species (SO_4^{2-}, NO_3^-, NH_4^+, OC, BC, sea salt, and mineral dust).

2007, while the value simulated in the CACTUS model was 0.92 (higher by ~7%). The model bias in AAOD is likely caused by the underestimation of BC concentrations.

3.2. Impacts of the emission inventories for 2006

3.2.1. Surface-layer aerosol concentrations

Table 4 presents the uncertainties in the aerosol surface-layer concentrations due to the emission differences in CACTUS. The primary particulates of BC and POA had approximately equivalent uncertainties in their concentrations (15.4% for BC and 11.1% for POA) and emissions (15.4% for BC and 11.9% for OC). The uncertainty in sulfate concentrations (3.9%) was close to the uncertainty in SO_2 emission (5.3%). Locations with high aerosol concentrations generally had lower uncertainties because the high polluted background air leaded to the fluctuation in concentration was not noticeable (Figs. 2 and 3).

Nitrate was different, with an uncertainty of 40.0% that was far higher than the emission uncertainties of 18.4% and 6.6% for NH_3 and NO_x, respectively. The nitrate chemistry is subject to sulfate formation in which SO_2 reacts preferentially with NH_3 and reduces ammonium nitrate

Table 4
Annual mean surface-layer aerosol concentrations (μg m^{-3}) averaged over eastern China (100°–120°E, 24°–44°N) in the CACTUS model based on the four emission inventories. The bottom rows compare the uncertainties in the concentrations due to the differences in the four emission inventories with those in the ACCMIP models caused by the differences in chemical and physical processes.

Emission inventories	Sulfate	Nitrate	Ammonium	POA	SOA	BC
ACCMIP	6. 8	1.6	2.8	4.1	0.6	1.5
HTAP	7.5	5.0	4.4	3.4	0.5	1.2
EDGAR	7.9	3.5	4.0	3.4	0.6	1.2
INTEX-B	7.3	3.8	3.8	3.4	0.6	1.4
Emission[a]: Mean ± Std	7.6 ± 0.3	3.5 ± 1.4	3.8 ± 0.7	3.6 ± 0.4	0.6 ± 0.1	1.3 ± 0.2
Std/Mean × 100%	3.9%	40.0%	18.4%	11.1%	16.7%	15.4%
Model[b]: Mean ± Std	5.2 ± 1.7	1.6 ± 0.7	2.0 ± 1.7	4.1 ± 0.7	4.2 ± 0.8	1.4 ± 0.4
Std/Mean × 100%	32.7%	43.8%	85.0%	17.1%	19.0%	28.6%

[a] Uncertainties in the concentrations due to the differences in the four emission inventories.
[b] Uncertainties in the concentrations from the ACCMIP models due to the differences in chemical and physical processes.

Table 5
Annual mean aerosol column burdens (mg m^{-2}) averaged over eastern China (100°–120°E, 24°–44°N) in the CACTUS model based on the four emission inventories. The bottom rows compare the uncertainties in the column burdens due to the differences in the four emission inventories with those of the ACCMIP models caused by the differences in chemical and physical processes.

Emission inventories	Sulfate	Nitrate	Ammonium	POA	SOA	BC
ACCMIP	10.7	1.5	3.8	4.5	1.2	1.5
HTAP	11.4	4.3	5.5	3.9	1.2	1.2
EDGAR	12.5	3.1	5.2	4.1	1.3	1.2
INTEX-B	12.2	3.2	5.1	3.5	1.1	1.3
Emission[a]: Mean ± Std	11.7 ± 0.8	3.0 ± 1.2	4.9 ± 0.8	4.0 ± 0.4	1.2 ± 0.1	1.3 ± 0.1
Std/Mean × 100%	6.8%	40.0%	16.3%	10.0%	8.3%	7.7%
Model[b]: Mean ± Std	11.9 ± 3.4	9.2 ± 8.7	4.0 ± 2.1	5.1 ± 0.8	5.0 ± 0.9	1.7 ± 0.8
Std/Mean × 100%	28.6%	94.6%	52.5%	15.7%	18.0%	47.1%

[a] Uncertainties in the column burdens due to the differences in the four emission inventories.
[b] Uncertainties in the column burdens from the ACCMIP models due to the differences in chemical and physical processes.

production. As a result, nitrate had a high uncertainty in eastern China, coexisting with high concentrations of sulfate. Besides, NH_3 emission affects nitrate production at large. The ACCMIP inventory had the lowest NH_3 emission and halved the nitrate concentration (1.6 μg m^{-3}) compared to other emission inventories. The HTAP inventory had the largest NH_3 emission and resulted in the maximum nitrate concentration (5.0 μg m^{-3}). There was a maximum uncertainty in nitrate in northwestern China because the nitrate fluctuation stood out in the clean atmosphere and because the uncertainty of NH_3 emission over that location was moderate (Fig. 1).

Compared with the results of the ACCMIP models, the differences in surface-layer concentrations due to emissions were small. This is in agreement with the conclusion of the global case by Textor et al. (2007). The surface-layer nitrate concentration had an uncertainty of 40.0% due to emissions, which is comparable to the uncertainty of 43.8% due to the model difference. An optimal nitrate simulation requires both improvements in emissions and the model.

3.2.2. Aerosol column burdens

Aerosol column burdens had geographical distributions that followed the surface-layer concentrations (figure not shown), and the uncertainties were primarily attributed to differences in the models themselves (Table 5). The uncertainty in the nitrate burden (40%) equaled the uncertainty at the surface at which the maximum concentration was located. The uncertainty in the nitrate burden due to the ACCMIP model difference, however, was up to 94.6% because a few models (e.g., GISS-E2-R, STOC-HadAM3) lofted ammonia in convective plumes at tropical sources and produced unexpectedly high nitrate concentrations in the upper troposphere (Shindell et al., 2013). Discrepancy in the vertical nitrate distribution enlarges the diversity of model results.

3.2.3. Optical properties of aerosols

Natural aerosols are independent of the emission inventories and were removed from this discussion. As shown in Table 6, the ACCMIP inventory produced the lowest concentrations of sulfate and nitrate and consequently led to the smallest fAOD (0.25). The uncertainty in the fAOD from emissions was 10.0%, corresponding to one standard deviation (0.03). This deviation is small because it is only one fifth of the standard deviation of the fAOD across the ACCMIP models and is smaller than the minimum uncertainty (0.05) of the MODIS AOD over land (Remer et al., 2005). Removing the mineral dust effect, the AAOD relevant to the fine-mode particulates was 0.011, which is half less than the total AAOD (0.027) in Section 3.1.2. The corresponding deviation is less to 0.001 with the uncertainty of 9.0%. Because low AAOD benefits low AOD and vice visa, their contemporary change makes the uncertainty in SSA quiet small (1%).

The geographical distributions of uncertainties in optical properties were similar to the anthropogenic aerosols and the total aerosol particulates. As shown in Fig. 4, the total AOD and SSA had high uncertainties in eastern China, illustrating their sensitivity to changes in aerosol column burdens and the BC fraction. The AAOD was rather uncertain in India due to the strong local biomass burnings and also along the southern coast of China likely due to the downwind transportation of BC particulates from biomass burning in the Indochina Peninsula.

3.2.4. Direct radiative forcing of aerosols

Table 7 shows the annual mean instantaneous DRF by anthropogenic aerosols (ammonium sulfate, ammonium nitrate, POA, SOA and BC) between 1850 and 2006 over eastern China. We report the radiative forcing under both clear-sky and all-sky conditions because the presence of thick optical clouds above aerosols weakens the aerosol DRF and bright clouds enhance aerosol absorption above it.

Table 6
Annual single scattering albedo (SSA), absorption aerosol optical depth (AAOD) and fine-mode aerosol optical depth (fAOD) at 550 nm associated with anthropogenic (Anth.) aerosols in the CACTUS model with the four-year 2006 emission inventories. The impacts of mineral dust are not included. All of the values were averaged over eastern China (100°E–120°E, 24°N–44°N). The bottom rows compare the uncertainties in the optical properties due to the differences in the four emission inventories with those in the ACCMIP models caused by the differences in chemical and physical processes.

Emission inventories	Anth. SSA	Anth. AAOD	fAOD		
			No assimilation	Assimilated MODIS fAOD	Assimilated MISR fAOD
ACCMIP	0.95	0.013	0.25	0.27	0.25
HTAP	0.97	0.010	0.32	0.33	0.31
EDGAR	0.97	0.010	0.31	0.31	0.30
INTEX-B	0.96	0.011	0.30	0.31	0.29
Emission[a]: Mean ± Std	0.96 ± 0.01	0.011 ± 0.001	0.30 ± 0.03	0.31 ± 0.03	0.29 ± 0.03
Std/|Mean| × 100%	1.0%	9.0%	10.0%	9.7%	10.3%
Model[b]: Mean ± Std	0.93 ± 0.04	0.021 ± 0.007	0.27 ± 0.15		
Std/|Mean| × 100%	4.3%	33.3%	55.6%		

[a] Uncertainties in the aerosol optical properties due to the differences in the four emission inventories.
[b] Uncertainties in the aerosol optical properties from the ACCMIP models due to the differences in chemical and physical processes.

Table 7
Anthropogenic aerosol direct forcings (Wm^{-2}) between 1850 and 2006 and their uncertainties due to the four-year 2006 emission inventories. Also shown are aerosol direct forcings between 1850 and 2000 recalculated based on aerosol dry mass concentrations from the ACCMIP models. All of the forcing values were averaged over eastern China (100°E–120°E, 24°N–44°N).

	Clear-sky			All-sky		
	No assimilation	Assimilated MODIS fAOD	Assimilated MISR fAOD	No assimilation	Assimilated MODIS fAOD	Assimilated MISR fAOD
TOA forcing						
Emission[a]: Mean ± Std	−6.95 ± 1.20	−7.28 ± 1.13	−6.92 ± 1.09	−3.63 ± 0.84	−3.83 ± 0.84	−3.67 ± 0.81
Std/|Mean| × 100%	17.3%	15.5%	15.8%	23.1%	21.9%	22.1%
Model[b]: Mean ± Std	−4.87 ± 1.36			−1.31 ± 1.37		
Std/|Mean| × 100%	27.9%			104.5%		
Atmospheric forcing						
Emission[a]: Mean ± Std	4.36 ± 0.52	4.62 ± 0.76	4.24 ± 0.73	3.91 ± 0.47	4.10 ± 0.70	3.74 ± 0.67
Std/|Mean| × 100%	11.9%	16.5%	17.2%	12.0%	17.1%	17.9%
Model[b]: Mean ± Std	7.56 ± 3.76			7.10 ± 3.66		
Std/|Mean| × 100%	49.7%			51.5%		
Surface forcing						
Emission[a]: Mean ± Std	−11.31 ± 0.68	−11.90 ± 0.38	−11.15 ± 0.38	−7.54 ± 0.37	−7.93 ± 0.15	−7.41 ± 0.14
Std/|Mean| × 100%	6.0%	3.2%	3.4%	4.9%	1.9%	1.9%
Model[b]: Mean ± Std	−12.43 ± 3.73			−8.41 ± 2.70		
Std/|Mean| × 100%	30.0%			32.1%		

[a] Uncertainties in the concentrations due to the differences in the four emission inventories.
[b] Uncertainties in the aerosol DRF in the CACTUS model using the dry mass concentrations of sulfate, nitrate, OA and BC from the ACCMIP models.

Fig. 5 shows the geographical distribution of clear-sky DRF and its uncertainty. The all-sky forcing map is not shown because it is similar to the clear-sky DRF. The aerosol DRF attained a maximum in the northern region of eastern China. Atmospheric forcing and surface forcing showed relatively low uncertainties over eastern China where their forcing values were high. The aerosol DRF at the top of the atmosphere (TOA) is the small difference between the two large forcings in air and at the surface, and showed a high uncertainty along with the maximum forcing value.

The regional TOA DRF exceeded the global aerosol DRF (−0.35 W m^{-2}) between 1750 and 2011 (Myhre et al., 2013a). In clear-sky conditions, the regional TOA DRF was −6.95 W m^{-2} with a standard deviation of 1.20 W m^{-2}. Cloud cover weakened the TOA forcing down to −3.63 W m^{-2} with a lesser standard deviation of 0.84 W m^{-2}. The decreased mean forcing values suppressed the forcing variation. However, the DRF uncertainty was 17.3% in clear-sky conditions and increased up to 23.1% in all-sky conditions. The larger uncertainty with the presence of clouds agrees with the AeroCOM finding that, due to the model differences, the all-sky aerosol DRF in the phase I models had a larger uncertainty of 72% (56% in phase II models) compared with the clear-sky DRF uncertainty of 35% (27% in phase II models) (Schulz et al., 2006; Myhre et al., 2013b).

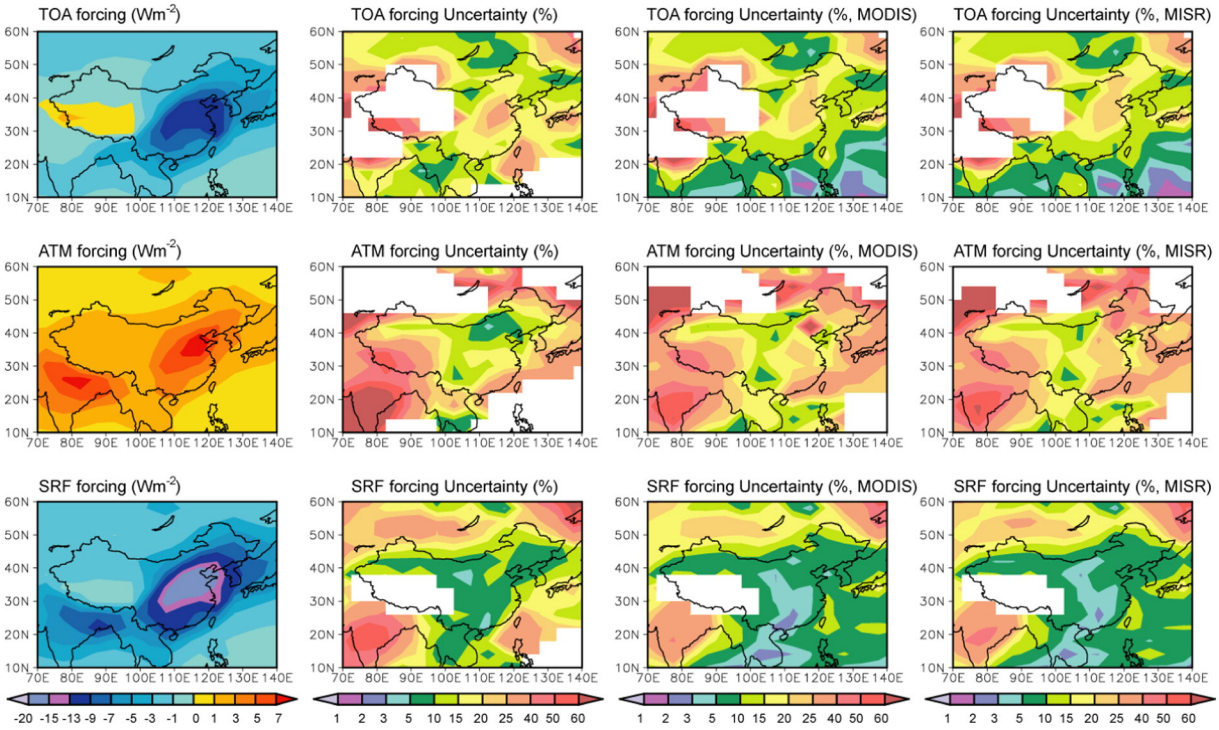

Fig. 5. Simulated annual mean clear-sky anthropogenic aerosol direct radiative forcing (Wm^{-2}) at the top of atmosphere (TOA), in the atmosphere (ATM) and at the surface (SRF) between 1850 and 2006 (the 1st column) averaged over the emission inventories of ACCMIP, HTAP, EDGAR and INTEX-B. The 2nd, 3rd, and 4th columns are the uncertainties (ratio of the standard deviation to the mean value as a percentage) in the direct radiative forcings without the assimilation of AOD, with assimilated MODIS AOD, and with assimilated MISR AOD, respectively. The white areas in the panels are locations of aerosol direct forcing that was less than 0.5 Wm^{-2} in which the uncertainties were quiet large; these were masked out for clarity.

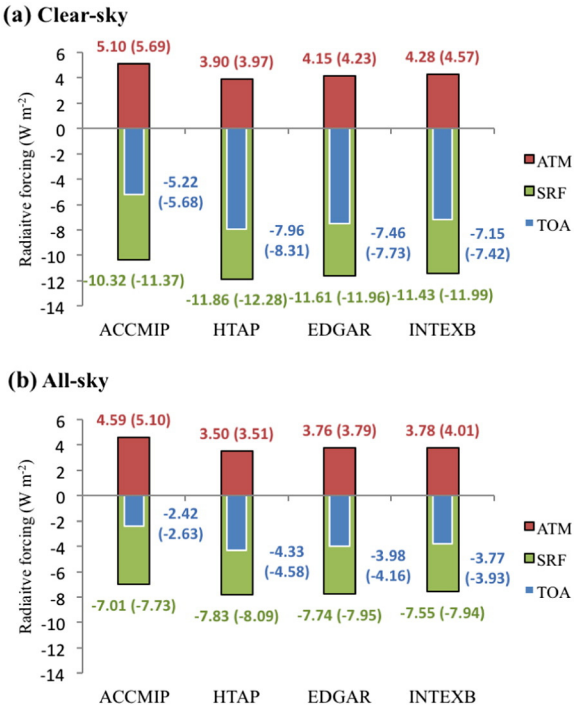

Fig. 6. Annual anthropogenic aerosol direct radiative forcing (Wm^{-2}) at the top of the atmosphere (TOA), in the atmosphere (ATM) and at the surface (SRF) between 1850 and 2006 averaged over eastern China (100°E–120°E, 24°N–44°N),with each of the emission inventories of ACCMIP, HTAP, EDGAR and INTEX-B. The forcing values in parentheses are from simulations with the MODIS fAOD assimilation, and the rest are from the simulations without assimilation.

We recalculated the anthropogenic aerosol DRF from the ACCMIP aerosol mass concentrations within the CACTUS radiation module. Again, the regional uncertainty in aerosol DRF was more sensitive to the model differences than the emissions (Table 7). Besides, compared to the uncertainties in global mean radiative forcing due to the differences in emissions, the uncertainties in regional mean forcing were stronger. The global mean DRF values at the TOA were -0.70 ± 0.04 Wm^{-2} (6.4%) in clear-sky and -0.37 ± 0.03 Wm^{-2} (8.8%) under all-sky conditions, while the values over eastern China were -6.95 ± 1.20 Wm^{-2} (17.3%) and -3.63 ± 0.84 Wm^{-2} (23.1%), respectively.

CACTUS basically captured the total AOD but the anthropogenic AOD may still be biased. Assimilating MODIS fAOD slightly increased the model fAOD (Table 6) and strengthened the mean aerosol DRF under clear- and cloudy-sky conditions by approximately 5% (Table 7). The MISR AOD had a systematically lower AOD than the actual value (Liu et al., 2010) and could not significantly adjust the fAOD and DRF. Furthermore, in spite of the changes in the mean values, neither of the fAOD assimilations could substantially reduce the model uncertainties, likely because the observation error of AOD was larger when the AOD value was higher (see the MODIS retrieval uncertainty in Section 2.4), which discounted the effectiveness of assimilation.

Fig. 6 shows the aerosol DRF over eastern China based on the four emissions inventories. The regional all-sky TOA DRF ranged from -2.4 Wm^{-2} with the ACCMIP emissions to -4.3 Wm^{-2} with the HTAP emissions, and, after AOD assimilation, the forcings were between -2.6 Wm^{-2} and -4.6 Wm^{-2}, always at twice the difference. Zhuang et al. (2013) discussed the impact of aerosol mixing of state and lateral boundary conditions on aerosol DRF in regional models. They showed that the TOA DRF ranged from -5.24 Wm^{-2} to -4.95 Wm^{-2} in clear-sky and -0.78 Wm^{-2} to -0.61 Wm^{-2} in all-sky over China. These deviation ranges are smaller than the differences induced by emissions in the present study, suggesting the importance of an accurate emission inventory in aerosol simulation.

4. Discussions on the impact of AAOD assimilation

In previous section we have calculated aerosol radiative forcing by using assimilated AOD. It would be ideal to have assimilated AAOD in forcing calculation, but it is difficult to estimate error in observed AAOD (parameter e_o in Eq. (3)). Here we can test an extreme situation by assuming AAOD had no measurement error. Thus, the discussions of AAOD assimilation here are qualitative.

Table 8 compares the effects of the fAOD assimilation alone with those when both fAOD and AAOD were assimilated under clear-sky conditions. The assimilation was based on the MODIS and OMI datasets. With assimilation of both fAOD and AAOD, simulated aerosol DRF was stronger in the atmosphere and at the surface. The assimilation of AAOD increased AAOD in the model and allowed more sunlight to become trapped in the air. It enhanced atmospheric warming and weakened the TOA cooling. The uncertainty in the atmospheric forcing decreased from 16.5% to 7.3%, but that in surface forcing increased from 3.2% to 5%. Compared to the result with fAOD assimilation alone, the assimilation of AAOD reduced the uncertainty in the TOA forcing from 15.5% to 14.4%. Because we ignored the large error in AAOD observations, the realistic impact of AAOD assimilation should be smaller than the impact reported here.

5. Conclusions

This study assessed the impact of uncertainties in four emission inventories, ACCMIP, HTAP, EDGAR and INTEX-B, on anthropogenic aerosol fields over eastern China within the global chemistry–aerosol–climate model. Those inventory lacking certain emission species or sectors were combined with other inventories. We defined the uncertainty as the percentage of the standard deviation divided by the mean value across the simulations with the inventories. Over eastern China (100°–120°E, 24°–44°N), the emission uncertainties in SO_2, NH_3, NO_x CO, OC, and BC in the simulations were 5.3%, 18.4%, 6.6%, 27.9%, 11.9% and 15.4%, respectively.

The uncertainties in surface-layer aerosol concentrations in eastern China due to the four emission inventories were 3.9%, 40.0%, 18.4%,

Table 8
Impacts of AAOD assimilation to the anthropogenic aerosol DRF under clear-sky conditions between 1850 and 2006 averaged over eastern China (100°E–120°E, 24°N–44°N).

	No Assimilation	Assimilated MODIS fAOD	Assimilated MODIS fAOD + OMI AAOD
TOA forcing			
Emission: Mean ± Std	-6.95 ± 1.20	-7.28 ± 1.13	-7.03 ± 1.01
Std/|Mean| × 100%	17.3%	15.5%	14.4%
Atmospheric forcing			
Emission: Mean ± Std	4.36 ± 0.52	4.62 ± 0.76	5.34 ± 0.39
Std/|Mean| × 100%	11.9%	16.5%	7.3%
Surface forcing			
Emission: Mean ± Std	-11.31 ± 0.68	-11.90 ± 0.38	-12.36 ± 0.62
Std/|Mean| × 100%	6.0%	3.2%	5.0%

11.1%, 16.7%, and 15.4% for sulfate, nitrate, ammonium, POA, SOA, and BC, respectively. The high uncertainty in nitrate concentration is due to the complex nitrate chemistry and the uncertainty in NH_3 emissions. The aerosol column burdens have comparable uncertainties to the surface-layer concentrations from emissions, both of which are smaller than those due to the model differences in chemical and physical processes. The regional surface-layer nitrate concentration had an exceptionally high uncertainty of 40.0% in emissions, which is comparable to the uncertainty of 43.8% across the ACCMIP models with a unified emission inventory.

Due to the emission differences, the uncertainties in fAOD and AAOD were 10% and 9%, and those in the TOA aerosol DRFs were 17.3% ($-6.95 \pm 1.20\ Wm^{-2}$) and 23.1% ($-3.63 \pm 0.84\ Wm^{-2}$) over eastern China. Both the forcing magnitudes and uncertainties were stronger than the global mean values of $-0.70 \pm 0.04\ Wm^{-2}$ (6.4%) under clear-sky and $-0.37 \pm 0.03\ Wm^{-2}$ (8.8%) under all-sky conditions, respectively. Compared to the MISR fAOD, the assimilation of the MODIS fAOD was more effective in enhancing the aerosol DRF. On an annual and regional mean basis, the all-sky DRF at the TOA ranged from $-2.4\ Wm^{-2}$ with the ACCMIP inventory to $-4.3\ Wm^{-2}$ with the HTAP inventory. This doubled forcing highlights the importance of accurate emission inventories. After the MODIS AOD assimilation, the range limits changed to $-2.6\ Wm^{-2}$ and $-4.6\ Wm^{-2}$, respectively. However, due to the fAOD uncertainty in observations, the assimilation had limited effects in reducing the DRF uncertainty.

Overall, simulated aerosol concentrations showed low biases with all of the four emission inventories. In terms of simulated aerosol concentrations in China, it is hard to conclude which emission inventory is the best, because the biases in simulated aerosol concentrations vary with aerosol species. For example, simulated aerosol concentrations with the ACCMIP inventory showed the largest low biases in concentrations of sulfate and nitrate whereas the smallest low bias in concentrations of POA. In terms of simulated aerosol DRF, the HTAP emission inventory is found to lead to the strongest radiative forcing at the TOA and surface.

There are a few limitations to this research. Comparisons with the CAWNET aerosol measurements indicate an aerosol underestimation in CACTUS. The negative biases are associated with the missing subgrid pollutant variations in the model resolution and the potential model deficiency in chemistry. A regional model with advanced chemistry will be able to describe the emission impact in more detail. Seasonal variations are particularly important for NH_3 and BC in China, but these variations were ignored in CACTUS and should be investigated in the future.

Acknowledgements

This work has been supported by the National Basic Research Program of China (973 Program, 2010CB950804) and the Strategic Priority Research Program of the Chinese Academy of Sciences (Grant No. XDA05100503).

References

Chang, W., Liao, H., Wang, H., 2009. Climate responses to direct radiative forcing of anthropogenic aerosols, tropospheric ozone, and long-lived greenhouse gases in Eastern China over 1951–2000. Adv. Atmos. Sci. 26 (4), 748–762. http://dx.doi.org/10.1007/s00376-009-9032-4.

Cheng, T., Chen, H., Gu, X., Yu, T., Guo, J., Guo, H., 2012. The inter-comparison of MODIS, MISR and GOCART aerosol products against AERONET data over China. J. Quant. Spectrosc. Radiat. Transf. 113, 2135–2145. http://dx.doi.org/10.1016/j.jqsrt.2012.06.016.

Chung, C.E., Ramanathan, V., Carmichael, G., Kulkarni, S., Tang, Y., Adhikary, B., Leung, L.R., Qian, Y., 2010. Anthropogenic aerosol radiative forcing in Asia derived from regional models with atmospheric and aerosol data assimilation. Atmos. Chem. Phys. 10, 6007–6024. http://dx.doi.org/10.5194/acp-10-6007-2010.

Collins, W.D., Rasch, P.J., Eaton, B.E., Khattatov, B.V., Lamarque, J.F., Zender, C.S., 2001. Simulating aerosols using a chemical transport model with assimilation of satellite aerosol retrievals: Methodology for INDOEX. J. Geophys. Res. 106 (D7), 7313–7336.

Giorgi, Bi, X., Qian, Y., 2002. Direct radiative forcing and regional climatic effects of anthropogenic aerosols over East Asia: a regional coupled climate-chemistry/aerosol model study. J. Geophys. Res. 107 (D20), 4439. http://dx.doi.org/10.1029/2001jd001066.

Goto, D., Schutgens, N.A.J., Nakajima, T., Takemura, T., 2011. Sensitivity of aerosol to assumed optical properties over Asia using a global aerosol model and AERONET. Geophys. Res. Lett. 38, L17810. http://dx.doi.org/10.1029/2011GL048675.

Granier, C., Bessagnet, B., Bond, T., D'Angiola, A., van der Gon, H.D., Frost, G.J., Heil, A., Kaiser, J.W., Kinne, S., Klimont, Z., Kloster, S., Lamarque, J.-F., Liousse, C., Masui, T., Meleux, F., Mieville, A., Ohara, T., Raut, J.-C., Riahi, K., Schultz, M.G., Smith, S.J., Thompson, A., van Aardenne, J., van der Werf, G.R., van Vuuren, D.P., 2011. Evolution of anthropogenic and biomass burning emissions of air pollutants at global and regional scales during the 1980–2010 period. Clim. Chang. 109, 163–190. http://dx.doi.org/10.1007/s10584-011-0154-1.

Hansen, J., Lacis, A., Russell, G., Stone, P., Fung, I., Ruedy, R., Lerner, J., 1984. Climate sensitivity: Analysis of feedback mechanisms. In: Hansen, J.E., Takahashi, T. (Eds.), Climate Processes and Climate SensitivityGeophys. Monogr. Ser. vol. 29. AGU, Washington, D. C., pp. 130–163.

Huang, X., Song, Y., Li, M., Li, J., Huo, Q., Cai, X., Zhu, T., Hu, M., Zhang, H., 2012. A high-resolution ammonia emission inventory in China. Global Biogeochem. Cycles 26. http://dx.doi.org/10.1029/2011gb004161.

Kinne, S., Schulz, M., Textor, C., Guibert, S., Balkanski, Y., Bauer, S.E., Berntsen, T., Berglen, T.F., Boucher, O., Chin, M., Collins, W., Dentener, F., Diehl, T., Easter, R., Feichter, J., Fillmore, D., Ghan, S., Ginoux, P., Gong, S., Grini, A., Hendricks, J.E., Herzog, M., Horowitz, L., Isaksen, I., Iversen, T., Kirkevåg, A., Kloster, S., Koch, D., Kristjansson, J.E., Krol, M., Lauer, A., Lamarque, J.F., Lesins, G., Liu, X., Lohmann, U., Montanaro, V., Myhre, G., Penner, J.E., Pitari, G., Reddy, S., Seland, O., Stier, P., Takemura, T., Tie, X., 2006. An AeroCom initial assessment-optical properties in aerosol component modules of global models. Atmos. Chem. Phys. 6, 1815–1834.

Lamarque, J.-F., Bond, T.C., Eyring, V., Granier, C., Heil, A., Klimont, Z., Lee, D., Liousse, C., Mieville, A., Owen, B., Schultz, M.G., Shindell, D., Smith, S.J., Stehfest, E., Van Aardenne, J., Cooper, O.R., Kainuma, M., Mahowald, N., McConnell, J.R., Naik, V., Riahi, K., van Vuuren, D.P., 2010. Historical (1850–2000) gridded anthropogenic and biomass burning emissions of reactive gases and aerosols: methodology and application. Atmos. Chem. Phys. 10, 7017–7039. http://dx.doi.org/10.5194/acp-10-7017-2010.

Lamarque, J.-F., Shindell, D.T., Josse, B., Young, P.J., Cionni, I., Eyring, V., Bergmann, D., Cameron-Smith, P., Collins, W.J., Doherty, R., Dalsoren, S., Faluvegi, G., Folberth, G., Ghan, S.J., Horowitz, L.W., Lee, Y.H., MacKenzie, I.A., Nagashima, T., Naik, V., Plummer, D., Righi, M., Rumbold, S.T., Schulz, M., Skeie, R.B., Stevenson, D.S., Strode, S., Sudo, K., Szopa, S., Voulgarakis, A., Zeng, G., 2013. The Atmospheric Chemistry and Climate Model Intercomparison Project (ACCMIP): overview and description of models, simulations and climate diagnostics. Geosci. Model Dev. 6, 179–206. http://dx.doi.org/10.5194/gmd-6-179-2013.

Lee, L.A., Carslaw, K.S., Pringle, K.J., Mann, G.W., Spracklen, D.V., 2011. Emulation of a complex global aerosol model to quantify sensitivity to uncertain parameters. Atmos. Chem. Phys. 11, 12253–12273. http://dx.doi.org/10.5194/acp-11-12253-2011.

Lee, Y.H., Lamarque, J.-F., Flanner, M.G., Jiao, C., Shindell, D.T., Berntsen, T., Bisiaux, M.M., Cao, J., Collins, W.J., Curran, M., Edwards, R., Faluvegi, G., Ghan, S., Horowitz, L.W., McConnell, J.R., Ming, J., Myhre, G., Nagashima, T., Naik, V., Rumbold, S.T., Skeie, R.B., Sudo, K., Takemura, T., Thevenon, F., Xu, B., Yoon, J.-H., 2013. Evaluation of preindustrial to present-day black carbon and its albedo forcing from Atmospheric Chemistry and Climate Model Intercomparison Project (ACCMIP). Atmos. Chem. Phys. 13, 2607–2634. http://dx.doi.org/10.5194/acp-13-2607-2013.

Lei, Y., Zhang, Q., He, K.B., Streets, D.G., 2011. Primary anthropogenic aerosol emission trends for China, 1990–2005. Atmos. Chem. Phys. 11, 931–954. http://dx.doi.org/10.5194/acp-11-931-2011.

Li, J., Wang, W.-C., Liao, H., 2014. Past and future direct radiative forcing of nitrate aerosol in East Asia. Theor. Appl. Climatol. http://dx.doi.org/10.1007/s00704-014-1249-1.

Liao, H., Seinfeld, J.H., 2005. Global impacts of gas-phase chemistry-aerosol interactions on direct radiative forcing by anthropogenic aerosols and ozone. J. Geophys. Res. 110, D18208. http://dx.doi.org/10.1029/2005JD005907.

Liao, H., Seinfeld, J.H., Adams, P.J., Mickley, L.J., 2004. Global radiative forcing of coupled tropospheric ozone and aerosols in a unified general circulation model. J. Geophys. Res. 109 (D16207). http://dx.doi.org/10.1029/2003JD004456.

Liao, H., Chen, W.-T., Seinfeld, J.H., 2006. Role of climate change in global predictions of future tropospheric ozone and aerosols. J. Geophys. Res. 111, D12304. http://dx.doi.org/10.1029/2005JD006852.

Liao, H., Zhang, Y., Chen, W.-T., Raes, F., Seinfeld, J.H., 2009. Effect of chemistry–aerosol–climate coupling on predictions of future climate and future levels of tropospheric ozone and aerosols. J. Geophys. Res. 114, D10306. http://dx.doi.org/10.1029/2008JD010984.

Liu, J., Xia, X., Li, Z., Wang, P., Min, M., Hao, W., Wang, Y., Xin, J., Li, X., Zheng, Y., Chen, Z., 2010. Validation of multi-angle imaging spectroradiometer aerosol products in China. Tellus 62B, 117–124. http://dx.doi.org/10.1111/j.1600-0889.2009.00450.x.

Lu, Z., Streets, D.G., Zhang, Q., Wang, S., Carmichael, G.R., Cheng, Y.F., Wei, C., Chin, M., Diehl, T., Tan, Q., 2010. Sulfur dioxide emissions in China and sulfur trends in East Asia since 2000. Atmos. Chem. Phys. 10, 6311–6331. http://dx.doi.org/10.5194/acp-10-6311-2010.

Myhre, G., Myhre, A., Stordal, F., 2001. Historical evolution of radiative forcing of climate. Atmos. Environ. 35 (13), 2361–2373. http://dx.doi.org/10.1016/S1352-2310(00)00531-8.

Myhre, G., Shindell, D., Bréon, F.-M., Collins, W., Fuglestvedt, J., Huang, J., Koch, D., Lamarque, J.-F., Lee, D., Mendoza, B., Nakajima, T., Robock, A., Stephens, G., Takemura, T., Zhang, H., 2013a. Anthropogenic and natural radiative forcing. In: Stocker, T.F., Qin, D., Plattner, G.-K., Tignor, M., Allen, S.K., Boschung, J., Nauels, A., Xia, Y., Bex, V., Midgley, P.M. (Eds.), Climate Change 2013: The Physical Science

Basis. Contribution of Working Group I to the Fifth Assessment Report of the Intergovernmental Panel on Climate Change. Cambridge University Press, Cambridge, United Kingdom and New York, NY, USA, pp. 659–740.

Myhre, G., Samset, B.H., Schulz, M., Balkanski, Y., Bauer, S., Berntsen, T.K., Bian, H., Bellouin, N., Chin, M., Diehl, T., Easter, R.C., Feichter, J., Ghan, S.J., Hauglustaine, D., Iversen, T., Kinne, S., Kirkevåg, A., Lamarque, J.-F., Lin, G., Liu, X., Lund, M.T., Luo, G., Ma, X., van Noije, T., Penner, J.E., Rasch, P.J., Ruiz, A., Seland, Ø., Skeie, R.B., Stier, P., Takemura, T., Tsigaridis, K., Wang, P., Wang, Z., Xu, L., Yu, H., Yu, F., Yoon, J.-H., Zhang, K., Zhang, H., Zhou, C., 2013b. Radiative forcing of the direct aerosol effect from AeroCom Phase II simulations. Atmos. Chem. Phys. 13, 1853–1877. http://dx.doi.org/10.5194/acp-13-1853-2013.

Nakajima, T., Yoon, S.-C., Ramanathan, V., Shi, G.-Y., Takemura, T., Higurashi, A., Takamura, T., Aoki, K., Sohn, B.-J., Kim, S.-W., Tsuruta, H., Sugimoto, N., Shimizu, A., Tanimoto, H., Sawa, Y., Lin, N.-H., Lee, C.-T., Goto, D., Schutgens, N., 2007. Overview of the Atmospheric Brown Cloud East Asian Regional Experiment 2005 and a study of the aerosol direct radiative forcing in east Asia. J. Geophys. Res. 112, D24S91. http://dx.doi.org/10.1029/2007JD009009.

Nenes, A., Pilinis, C., Pandis, S.N., 1998. ISORROPIA: A new thermodynamic equilibrium model for multiphase multicomponent inorganic aerosols. Aquat. Geochem. 4, 123–152.

Ohara, T., Akimoto, H., Kurokawa, J., Horii, N., Yamaji, K., Yan, X., Hayasaka, T., 2007. An Asian emission inventory of anthropogenic emission sources for the period 1980–2020. Atmos. Chem. Phys. 7, 4419–4444. http://dx.doi.org/10.5194/acp-7-4419-2007.

Park, H., Chung, C.E., Ekman, A.M.L., Choi, J.-O., 2014a. Evaluation of ACCMIP simulated fine-mode AOD and its implication for aerosol direct forcing. Asia-Pac. J. Atmos. Sci. 50, 377–390. http://dx.doi.org/10.1007/s13143-014-0025-6.

Park, R.S., Lee, S., Shin, S.-K., Song, C.H., 2014b. Contribution of ammonium nitrate to aerosol optical depth and direct radiative forcing by aerosols over East Asia. Atmos. Chem. Phys. 14, 2185–2201. http://dx.doi.org/10.5194/acp-14-2185-2014.

Qin, Y., Xie, S.D., 2011. Estimation of county-level black carbon emissions and its spatial distribution in China in 2000. Atmos. Environ. 45, 6995–7004. http://dx.doi.org/10.1016/j.atmosenv.2011.09.017.

Remer, L.A., Kaufman, Y.J., Tanre, D., Mattoo, S., Chu, D.A., Martins, J.V., Li, R.-R., Ichoku, C., Levy, R.C., Kieidman, R.G., Eck, T.F., Vermote, E., Holben, B.N., 2005. The MODIS aerosol algorithm, products, and validation. J. Atmos. Sci. 62, 947–973.

Schulz, M., Textor, C., Kinne, S., Balkanski, Y., Bauer, S., Berntsen, T., Berglen, T., Boucher, O., Dentener, F., Guibert, S., Isaksen, I.S.A., Iversen, T., Koch, D., Kirkevåg, A., Liu, X., Montanaro, V., Myhre, G., Penner, J.E., Pitari, G., Reddy, S., Seland, Ø., Stier, P., Takemura, T., 2006. Radiative forcing by aerosols as derived from the AeroCom present-day and pre-industrial simulations. Atmos. Chem. Phys. 6, 5225–5246.

Shindell, D.T., Lamarque, J.-F., Schulz, M., Flanner, M., Jiao, C., Chin, M., Young, P.J., Lee, Y.H., Rotstayn, L., Mahowald, N., Milly, G., Faluvegi, G., Balkanski, Y., Collins, W.J., Conley, A.J., Dalsoren, S., Easter, R., Ghan, S., Horowitz, L., Liu, X., Myhre, G., Nagashima, T., Naik, V., Rumbold, S.T., Skeie, R., Sudo, K., Szopa, S., Takemura, T., Voulgarakis, A., Yoon, J.-H., Lo, F., 2013. Radiative forcing in the ACCMIP historical and future climate simulations. Atmos. Chem. Phys. 13, 2939–2974. http://dx.doi.org/10.5194/acp-13-2939-2013.

Stier, P., Feichter, J., Kloster, S., Vignati, E., Wilson, J., 2006. Emission-induced nonlinearities in the global aerosol system: results from the ECHAM5-HAM aerosol-climate model. J. Clim. 19, 3845–3862.

Streets, D.G., Bond, T., Carmichael, G.R., Fernandes, S.D., Fu, Q., He, D., Klimont, Z., Nelson, S.M., Tsai, N.Y., Wang, M.Q., Woo, J.H., Yarber, K.F., 2003. An inventory of gaseous and primary aerosol emissions in Asia in the year 2000. J. Geophys. Res. 108 (D21).

Textor, C., Schulz, M., Guibert, S., Kinne, S., Balkanski, Y., Bauer, S., Berntsen, T., Berglen, T., Boucher, O., Chin, M., Dentener, F., Diehl, T., Feichter, J., Fillmore, D., Ginoux, P., Gong, S., Grini, A., Hendricks, J., Horowitz, L., Huang, P., Isaksen, I.S.A., Iversen, T., Kloster, S., Koch, D., Kirkevåg, A., Kristjansson, J.E., Krol, M., Lauer, A., Lamarque, J.F., Liu, X., Montanaro, V., Myhre, G., Penner, J.E., Pitari, G., Reddy, M.S., Seland, Ø., Stier, P., Takemura, T., Tie, X., 2007. The effect of harmonized emissions on aerosol properties in global models — an AeroCom experiment. Atmos. Chem. Phys. 7, 4489–4501.

van Vuuren, D.P., Edmonds, J., Kainuma, M., Riahi, K., Thomson, A., Hibbard, K., Hurtt, G.C., Kram, T., Krey, V., Lamarque, J.-F., Masui, T., Meinshausen, M., Nakicenovic, N., Smith, S.J., Rose, S.K., 2011. The representative concentration pathways: an overview. Clim. Chang. 109, 5–31. http://dx.doi.org/10.1007/s10584-011-0148-z.

Wang, T.-J., Min, J.-Z., Xu, Y.-F., Lam, K.-S., 2003. Seasonal variations of anthropogenic sulfate aerosol and direct radiative forcing over China. Meteorol. Atmos. Phys. 84, 185–198. http://dx.doi.org/10.1007/s00703-002-0581-7.

Wang, L., Wang, Y., Xin, J., Li, Z., Wang, X., 2010a. Assessment and comparison of three years of Terra and Aqua MODIS Aerosol Optical Depth Retrieval (C005) in Chinese terrestrial regions. Atmos. Res. 97, 229–240. http://dx.doi.org/10.1016/j.atmosres.2010.04.004.

Wang, T., Li, S., Shen, Y., Deng, J., Xie, M., 2010b. Investigations on direct and indirect effect of nitrate on temperature and precipitation in China using a regional climate chemistry modeling system. J. Geophys. Res. 115. http://dx.doi.org/10.1029/2009jd013264.

Wang, Y., Xin, J., Li, Z., Wang, S., Wang, P., Hao, W.M., Nordgren, B.L., Chen, H., Wang, L., Sun, Y., 2011. Seasonal variations in aerosol optical properties over China. J. Geophys. Res. 116, D18209. http://dx.doi.org/10.1029/2010JD015376.

Wang, Y., Zhang, Q.Q., Jiang, J., Zhou, W., Wang, B., He, K., Duan, F., Zhang, Q., Philip, S., Xie, Y., 2014. Enhanced sulfate formation during China's severe winter haze episode in January 2013 missing from current models. J. Geophys. Res. Atmos. 119, 10,425–10,440. http://dx.doi.org/10.1002/2013JD021426.

Wu, J., Fu, C., Xu, Y., Tang, J.P., Wang, W., Wang, Z., 2008. Simulation of direct effects of black carbon aerosol and temperature and hydrological cycle in Asia by a Regional Climate Model. Meteorol. Atmos. Phys. 100, 179–193. http://dx.doi.org/10.1007/s00703-008-0302-y.

Xin, J., Wang, Y., Li, Z., Wang, P., Hao, W.M., Nordgren, B.L., Wang, S., Liu, G., Wang, L., Wen, T., Sun, Y., Hu, B., 2007. Aerosol optical depth (AOD) and Ångström exponent of aerosols observed by the Chinese Sun Hazemeter Network from August 2004 to September 2005. J. Geophys. Res. 112 (D05203). http://dx.doi.org/10.1029/2006JD007075.

Xin, J.Y., Wang, L.L., Wang, Y.S., Li, Z.Q., Wang, P.C., 2011. Trends in aerosol optical properties over the Bohai Rim in Northeast China from 2004 to 2010. Atmos. Environ. 45 (35), 6317–6325.

Yu, H., Kaufman, Y.J., Chin, M., Feingold, G., Remer, L.A., Anderson, T.L., Balkanski, Y., Bellouin, N., Boucher, O., Christopher, S., DeCola, P., Kahu, R., Koch, D., Loeb, N., Reddy, M.S., Schulz, M., Takemura, T., Zhou, M., 2006. A review of measurement-based assessments of the aerosol direct radiative effect and forcing. Atmos. Chem. Phys. 6, 613–666. http://dx.doi.org/10.5194/acp-6-613-2006.

Zhang, Y.H., Zhu, X.L., Slanina, S., Shao, M., Zeng, L.M., Hu, M., Bergin, M., Salmon, L., 2004. Aerosol pollution in some Chinese cities (IUPAC Technical Report). Pure Appl. Chem. 76 (6), 1227–1239.

Zhang, Q., Streets, D.G., Carmichael, G.R., He, K.B., Huo, H., Kannari, A., Klimont, Z., Park, I.S., Reddy, S., Fu, J.S., Chen, D., Duan, L., Lei, Y., Wang, L.T., Yao, Z.L., 2009. Asian emissions in 2006 for the NASA INTEX-B mission. Atmos. Chem. Phys. 9, 5131–5153.

Zhang, L., Liao, H., Li, J., 2010. Impacts of Asian summer monsoon on seasonal and interannual variations of aerosols over eastern China. J. Geophys. Res. 115, D00K05. http://dx.doi.org/10.1029/2009JD012299.

Zhang, H., Shen, Z., Wei, X., Zhang, M., Li, Z., 2012a. Comparison of optical properties of nitrate and sulfate aerosol and the direct radiative forcing due to nitrate in China. Atmos. Res. 113, 113–125. http://dx.doi.org/10.1016/j.atmosres.2012.04.020.

Zhang, H., Wang, Z., Wang, Z., Liu, Q., Gong, S., Zhang, X., Shen, Z., Lu, P., Wei, X., Che, H., Li, L., 2012b. Simulation of direct radiative forcing of aerosols and their effects on East Asian climate using an interactive AGCM-aerosol coupled system. Clim. Dyn. 38, 1675–1693. http://dx.doi.org/10.1007/s00382-011-1131-0.

Zhang, X.Y., Wang, Y.Q., Niu, T., Zhang, X.C., Gong, S.L., Zhang, Y.M., Sun, J.Y., 2012c. Atmospheric aerosol compositions in China: spatial/temporal variability, chemical signature, regional haze distribution and comparisons with global aerosols. Atmos. Chem. Phys. 12, 779–799. http://dx.doi.org/10.5194/acp-12-779-2012.

Zhao, Y., Nielsen, C.P., Lei, Y., McElroy, M.B., Hao, J., 2011. Quantifying the uncertainties of a bottom-up emission inventory of anthropogenic atmospheric pollutants in China. Atmos. Chem. Phys. 11, 2295–2308. http://dx.doi.org/10.5194/acp-11-2295-2011.

Zheng, B., Zhang, Q., Zhang, Y., He, K.B., Wang, K., Zheng, G.J., Duan, F.K., Ma, Y.L., Kimoto, T., 2015. Heterogeneous chemistry: a mechanism missing in current models to explain secondary inorganic aerosol formation during the January 2013 haze episode in North China. Atmos. Chem. Phys. 15, 2031–2049. http://dx.doi.org/10.5194/acp-15-2031-2015.

Zhou, Y., Cheng, S., Lang, J., Chen, D., Zhao, B., Liu, C., Xu, R., Li, T., 2015. A comprehensive ammonia emission inventory with high-resolution and its evaluation in the Beijing-Tianjin-Hebei (BTH) region, China. Atmos. Environ. 106, 305–317. http://dx.doi.org/10.1016/j.atmosenv.2015.01.069.

Zhuang, B.L., Jian, F., Wang, T.J., Li, S., Zhu, B., 2011. Investigation on the direct radiative effect of fossil fuel black carbon aerosol over China. Theor. Appl. Climatol. 104, 301–312. http://dx.doi.org/10.1007/s00704-010-0341-4.

Zhuang, B.L., Li, S., Wang, T.J., Deng, J.J., Xie, M., Yin, C.Q., Zhu, J.L., 2013. Direct radiative forcing and climate effects of anthropogenic aerosols with different mixing states over China. Atmos. Environ. 79, 349–361. http://dx.doi.org/10.1016/j.atmosenv.2013.07.004.